

## **Characterizing slope morphology using multifractal technique – a study from the western continental margin of India**

**Bishwajit Chakraborty, S.M. Karisiddaiah, A.A.A. Menezes, K. Haris, G. S. Gokul, W. Fernandes, G. Kavitha**  
CSIR-National Institute of Oceanography, Dona Paula, Goa: 403 004, India

**Abstract** Here we present the slope configuration of the submarine gullies, ridges and the adjacent slump zone off Goa, along the western continental margin of India (WCMI) utilizing multibeam bathymetric and single channel seismic data. The fluid flow migration signature in the form of pockmark seepages, traces of mud volcanoes and enhanced reflectors are observed in the area. Altogether thirty three depth profiles from the gully, ridge and slump areas depict downslope progression in gully incision and varying gradients in the gullies (1.19 - 4.07°) and ridges (2.13 - 3.70°), whereas the profiles of the slump zone are comparatively steady (2.25 - 2.51°). The scatter plot of the three slope characteristics viz., gradient, mean depth and root mean square (rms) relief, characterizes the profiles of the gullies, ridges and slump zone into three distinct clusters. Principal Component Analysis (PCA) as well corroborates the categorization. Furthermore, a stochastic multifractal technique has been employed to understand the nature of the fine-scale seafloor processes active in the slope region. The three estimated parameters of the depth profiles, i.e. the degree of multifractality ( $\alpha$ ), sparseness ( $C_1$ ), and the degree of smoothness ( $H$ ), substantiate a very high degree of multifractality for all the thirty-three bathymetric profiles. Except for the five adjacent profiles (four from the slump zone and one of the ridge), the remaining twenty-eight depth profiles of the gully, ridges and slump zones show negligible difference. Based on the multifractal study, we conclude that the observed discrimination might be due to the significant interaction between the bottom currents off Goa and the varied seafloor morphological aspects with seepages and faults.

**Keywords** Slope morphology, Gully, Slump, Pockmark, Multibeam and Multifractal technique.

**Corresponding Author:** Bishwajit Chakraborty

Email address: [bishwajit@nio.org](mailto:bishwajit@nio.org)

Telephone no.: 00-91-832-2450318

Fax no.: 00-91-832-2450692

## 1 Introduction

The slope morphology characterization and understanding the related processes through comprehensive usage of both the bathymetry and seismic data are relevant for the continental margin investigations (Mitchell 2005). Farre et al. (1983) have recognized two types of slope canyons whereas O'Grady et al. (2000) classified the continental slope shapes into distinct categories. Adams and Schlager (2000) proposed three basic slope profiles such as exponential, linear and gaussian types. Goff (2001) had shown significant variations in the passive continental margins. Green et al. (2007) quantitatively classified the shape of the slopes and inferred the role of erosional and depositional processes. Previous investigations using multibeam data analyses from the central part of the western continental margin of India (WCMI) involved both the semi-quantitative (Kodagali and Chakraborty 1993; Mukhopadhyay et al. 2008; Dandapath et al. 2010) and quantitative (Chakraborty et al. 2006; Dandapath et al. 2012) methods. In the present work, we utilized three parameters such as gradient, mean depth, and root mean square (rms) relief of the depth profiles to characterize the slope-confined gullies and ridges of the area on a wider perspective. Principal Component Analysis (PCA) has been used to determine the relationship among the seafloor parameters (Davis 1973). PCA is a mathematical procedure that uses an orthogonal transformation to convert a set of observations of possibly correlated variables into a set of values of uncorrelated variables called principal components. Here, PCA is being used to understand the interrelationship among the three parameters (gradient, RMS relief and depth) of the thirty three profiles chosen based on the three different slope morphological characteristics. However the PCA could not accomplish the fine scale analysis processes such as slumping or material flow in the slope region that may not be explained as observed in the present study. Therefore in order to overcome this uncertainty, we adopted a stochastic multifractal technique that has advantages to address the intermittency in the frame work of higher order non-linear dynamical system. In order to probe the intricacy of fine-scale roughness parameters of the depth profiles, employment of the higher order statistics is called for (Mandelbrot 1989).

Seafloor bathymetric data of the submerged objects have an extremely wide range of spatio-temporal scales, necessitating the application of the power law (Fox and Hayes 1985). The seafloor roughness has been dealt using fractal dimension (based on the power law exponent) of the depth data. Many of the fractals observed in nature have infinite hierarchy of statistical exponents that offer a convenient framework to quantify the complex systems (Dimri 2005). Therefore, complicated processes (with different scaling exponents) raveled from many interwoven fractal, subsets of time/space series, and similar processes are recognized as multifractal. It is essential to treat data related to the complicated processes as a scale invariant field and required exponent parameters rather than a unique scaling exponent (Hentschel and Procaccia 1983). An infinite number of fractal dimensions are sometimes needed to complete characterization of the scaling. In view of this, a stochastic

multifractal technique (Lovejoy et al. 2009) is implemented here to discriminate the fine-scale aspects within the thirty-three profiles.

In addition to the “introduction” section, there are four major sections that cover this entire work. The section on “methodology and regional settings” includes description of the WCMI seafloor morphology, multifractal characteristics and the regional setup including the circulation pattern and bottom currents. Likewise in the “results” section, seismic interpretation is used to explain subsurface details revealing the presence of pockmarks, pockmarked gully and a buried gully. Description of slope morphology and applications of multivariate analysis and stochastic multifractal analysis have also been included in this section. The section on the “discussion” describes the categorization of slope morphology at length and validation using PCA results, as well as addressing the intermittency in the nonlinear dynamical system, taking recourse to the stochastic multifractal technique. Finally, in the “conclusion” section, the overall findings have been recapitulated.

## **2 Methodology and regional settings**

### **2.1 Data for WCMI seafloor morphology**

Present work is based on the analyses of multi-beam bathymetric data coupled with the single channel seismic data acquired on-board RV Sindhu Sankalp and RV Gaveshani respectively. Medium depth high-resolution multibeam EM 302 system (Kongsberg Maritime, AS) operable at 30 kHz frequency was used during the survey. Important characteristics of the EM 302 system involve 150° angular coverage sector and 432 soundings per ping, and achievable swath width on a flat bottom is nearly five times the water depth. Equidistant space sounding mode was used for this survey. This is suitable for medium depth range between the 2-3000 m maintaining spatial resolution in terms of narrow beam-width ( $\sim 1^\circ \times 2^\circ$ ). The multibeam bathymetric data used in this study is acquired through the three short cruises of RV Sindhu Sankalp (SSK-17, SSK-23 and SSK-29) during the year 2011. The depth data files [stored as binary SIMRAD (raw data) - \*.all format] were post-processed using Neptune (Kongsberg Maritime, AS) and CFLOOR (Cfloor, AS) software for improved visualization including gridding (30 x 30 m). Besides, the geo-referenced data points containing depth values were imported to ArcGIS (Geographical Information System) developed by ESRI Inc. The data were then interpolated to raster using cubic convolution methods and subsequently high resolution images were generated. Cubic convolution tends to sharpen the data and is more accurate as compared to other methods such as bilinear interpolation etc. Corresponding profile lengths within 200 - 1200 m water depth across the shelf have been selected and the area with water depth up to 1900 m has been partitioned into northern and southern block (Figs. 1a and b).

The study area stretches over 5310 km<sup>2</sup> offshore Goa, and an average slope of 3.11<sup>0</sup>. Here, we describe gullies, ridges in the north, and slump towards the south within the quadrangle of 15°10' N to 16°20' N and 72°10'

E to 73°00' E. The combination of gullies, ridges and slumps have carved the shelf break and upper slope of the study area (Fig. 2). From the earlier studies/surveys in this region we have noted that there exist BSR (bottom simulating reflector) zone almost 50 km from the present study area (Fig .1a).

The determination of slope curvature was carried out by curve-fitting (Adams and Schlager 2000). And the quantitative analyses of average slope angle and rms relief relating to slope morphology was carried out following the techniques of Goff (2001) and Green et al. (2007) respectively. Here the slope angle is evaluated from each profile by the slope morphology. It is computed by taking the arctangent of the difference in mean depth over adjacent profile divided by the down-slope spacing of the profile. The rms relief represents square root of morphological variance as a function of depth. It measures the average variability about the mean value along each profile.

## 2.2 Multifractal characterization

There are two important formalisms of the multifractal analysis such as: i) “strange” chaotic attractors (Halsey et al. 1986) and ii) “stochastic” multifractal fields (Schertzer and Lovejoy 1987). The analyses of the multifractal distribution pattern in the “strange” attractors formalism is based on the box counting method, which engages the correlation dimension and multifractal spectrum related parameters. However the another formalism known as “stochastic” multifractal field allows quantification of the multifractal flux with just three fundamental parameters such as degree of multifractality ( $\alpha$ ), sparseness ( $C_1$ ) and degree of smoothness ( $H$ ) (Gagnon et al. 2006). The “stochastic” multifractal formalism has an advantage over common dimension multifractal formalism i.e., “strange” attractors (developed for low dimensional deterministic chaos applications). Seafloor topography can be modeled considering a small number of (generally deterministic) or many (stochastic) degrees of freedom (Cheng and Agterberg 1996; Chakraborty et al. 2013). In order to incorporate higher degree of freedom and variability over a wide range of scales, stochastic approaches are preferred as they have infinite-dimensional probability space. Moreover, another straightforward formalism known as “universal” multifractal (UM) (Seuront et al. 1999) can be considered under stochastic multifractal framework. UM covers statistical behavior of the fields from larger to smaller scales as well as from extreme to mean behavior (Lovejoy and Schertzer 2007).

One way to characterize the stochastic processes is to use its statistical moments. The statistical moment of a multifractal process is a power law that can be expressed as  $\langle \varphi_\lambda^q \rangle = \lambda^{K(q)}$ , where  $\varphi_\lambda$  is the scale by scale conserved multifractal flux,  $q$  is the order of the moment and  $\lambda = L/l$  ( where  $L$  and  $l$  represents largest and smallest scale in the data) is the scale ratio. The term  $K(q)$  is a nonlinear convex function which characterizes the scaling of the moments of the  $\varphi_\lambda$ , which is also known as a moment scaling function. With reference to the existence of a stable attractive multifractal processes, universal multifractal  $K(q)$  can be expressed as  $[= \{C_1/(\alpha - 1)\}(q^\alpha - q)]$ , where  $\alpha$  and  $C_1$  are the basic parameters characterizing the scaling properties of the multifractal flux  $\varphi_\lambda$ . The term  $\alpha$  shows the multifractality index, which varies from 0 to 2. For monofractal case,  $\alpha = 0$ , and  $\alpha = 2$  is

the log-normal case. This parameter describes how rapidly the fractal dimensions of sets at different thresholds vary as they leave the mean singularity.  $C_1$  is the codimension parameter of the set. Low  $C_1$  ( $\sim 0$ ), implies that the field is close to the mean value, and  $C_1$  ( $> 0$ ) indicates that the region contributing to the mean is a sparse fractal set. The term  $H$  can be interpreted as a degree of smoothness where higher  $H$  means smoother fields. If  $H = 0$ , the field is conserved (a stationary process). However, most fields observed in the nature are not conserved, and  $H$  specifies the exponent of power law filter (the order to fractional integration). Implementation of Fractionally Integrated Flux (FIF) model is needed in order to obtain a conserved field from the observed one for estimating the “stochastic” multifractal field parameters having greater spectral exponents ( $\beta \sim 2$ ). However, estimated  $\alpha$  and  $C_1$  parameters using FIF models may not be always accurate, because it shares a convolution characterized by the exponent  $H$ . Therefore to evaluate the conserved multifractal flux, application of trace moment analyses is necessary so that the differentiation is possible (i.e., taking the absolute value of the gradients). The trace moment algorithm is available at [http: www. physics.mcgill.ca ~eliasl/](http://www.physics.mcgill.ca/~eliasl/), which has been used for this purpose.

The detailed application of the “stochastic” multifractal for seafloor studies are discussed recently (Chakraborty et al. 2014). The first step to obtain  $\varphi_\lambda$  from the intensity field involves removal of  $\lambda^{-H}$  in the  $I_\lambda = \varphi_\lambda \lambda^{-H}$ . This is equivalent to a filtering as in Fourier space with power law, which is a scale invariant smoothing. On elimination of  $\lambda^{-H}$ , only the underlying conserved multifractal flux  $\varphi_\lambda$  is retained. The next step is to examine the scaling of the statistical moments of  $\varphi_\lambda$ . To this end, we normalize  $\varphi_\lambda$  so that the ensemble average of all the samples is  $\langle \varphi_\lambda \rangle = 1$ . Thereafter, the  $q^{\text{th}}$  power of the samples (bathymetry profile values) over the sets of size  $l = L/\lambda$  is determined. It gives the moments of the normalized multifractal flux for a given value of  $q$ . This procedure is performed for different values of  $q$ , and  $K(q)$  is evaluated from the logarithmic slopes. The multifractality of the field can be validated with nonlinear  $K(q)$  of the representative plots for thirty-three profiles comprising of gullies, ridge, and slumping zone. From the values of  $K(q)$ , the parameters  $C_1$  and  $\alpha$  are estimated using:  $C_1 = K'(1)$  and  $\alpha = K''(1)/K'(1)$ . The values of  $\alpha$  and  $C_1$  combined with  $\beta$  are used to estimate values of  $H$ :  $\beta = 1 + 2H - K(2)$ .

## 2.3 Regional set up

### 2.3.1 Slope characteristics

Tectonically western continental margin of India is a passive and divergent margin. The study area is dissected by NNW to SSE trending faults, fractures and a ridge system (Chakraborty et al. 2006; Mukhopadhyay et al. 2008, Bhattacharya and Chaubey 2001). On a regional scale along the western offshore of India one can see set of faults which are the older NNW-SSE trending tectonic elements parallel to the Dharwarian trend which has influenced the depositional pattern (Bhattacharyya et al. 2009). Besides, a series of parallel sets of longitudinal extension faults and NW-SE trending structural features (Laccadive ridge, Laxmi ridge, Prathap ridge complex, Panikkar ridge) abound the western offshore. Ramification and network of all these faults have virtually configured and molded the geomorphology of the study area. Some of these faults act as channel ways for the

migration of hydrocarbon gas and fluids (Singh et al 2011; Dandapath et al 2010, 2012). The shape of the WCMI reveals a wider shelf (345 km) and a narrow slope in the north compared to a narrow shelf (60 km) and a wider slope in the south (Karisiddaiah et al. 1993). Reineck and Singh (1980) concluded that the upper slope region being adjacent to shelf break/edge experiences complex hydrodynamic environment, which also affects sedimentological regime. Hovland et al. (2002) demonstrated the strength of bottom currents in modifying the seafloor shape including pockmarks. Current-controlled pockmarks as noticed in the adjacent study area (Dandapath et al. 2010) were also reported elsewhere (Bøe et al. 1998). Multi-beam bathymetric data of the study area show that the length of the gully is of variable dimension. Generally, gullies are steep-sided confined channels incised by surface or subsurface flow, and shown to be common features on the continental slopes (Spinelli and Field 2001), submarine canyon walls (Lastras et al. 2007), and delta slopes (Maillet et al. 2006). Submarine gullies also play a pivotal role in the general evolution of continental margins over relatively long periods of time (Field et al. 1999). Gullies are important agents of submarine erosion and downslope sediment transfer from the upper slope to the continental rise (Dowdeswell et al. 2008). They contribute to the facies of slope deposits (Syvitski et al. 1996), and also occasionally considered as an important architecture of the petroleum reservoirs (Hewlett and Jordan 1993). Studies on the WCMI have demonstrated that the slope region have been subjected to extensive slumping during the late Pleistocene Epoch (Stackelberg 1972; Shetty 1972; Hussain and Guptha 1985; Rao et al. 1988; Rao 1989; Guptha et al. 2002). These studies inferred that the slumping in the WCMI was set in motion during the Holocene. Holocene sedimentary processes in the area are controlled primarily by bottom topography and dynamics of the current regime. Although the late Pleistocene palaeo-topography appears as a basic factor in controlling the areal distribution of Holocene deposits, modern processes also have been influential (Karisiddaiah et al. 2002). Main controlling factor of slump appears to be due to the dissociation of adjacent underlying gas hydrates deposits (Fig. 1a) as reported by Rao et al. (2001).

### *2.3.2 Circulation Pattern*

Regional circulation is characterized by seasonal reversal of monsoon driven surface and bottom currents, summer upwelling and winter down-welling (Naqvi et al. 2010), create an unstable oceanographic condition over the area. A strong coast parallel (NNW-SSE trending) bottom current covering 40 km wide runs through the present study area (Shetye et al. 1990). Bottom currents often play a major role in the continental margin sedimentation. They can erode, mould, transport and redistribute the sediments supplied to the slope by downslope flows and vertical settings (Weaver et al. 2000). The bottom currents in WCMI move northward carrying low salinity water during the southwest monsoon (summer) and move southward carrying high salinity water during the northeast monsoon (winter). These currents are parallel to the bathymetric contours (~250 m). This suggests that the bottom currents actively participating in modifying the seafloor morphology indicating higher sediment deposition or erosion. Considering the current characteristics of Hernandez-Molina et al. (2011)

to our work, we propose that the circulation of water masses might lead to the development of the along-slope currents and generate erosion and depositional features within the gullies, ridges and slump zone. Stow et al. (2009) considers that the bottom currents mooring investigations using ADCP deployed off Goa continental margin revealed that there is a seasonal based strong poleward and equatorward currents ( $\sim 30$  cm/sec) off Goa slope. The magnitude of the currents is dominant towards the slope region of the southern end (Bhatkal) than the north (Jaigarh) (Amol et al. 2012). This diverse current pattern especially off Goa slope region appears to be one of the influencing factors in controlling and moulding the configuration of the slope morphology.

### 3 Results

#### 3.1 Seismic interpretation of the line tracks

Single channel seismic data (4.5 -8 kJ), (Fig. 3) can explain the subsurface details for understanding the linkage of pockmark gully and adjacent BSR zone. Besides, single channel seismic data from this study area can also provide detailed subsurface information. The seismic reflection profiles [Figs. 3a-f; L-(3-7)], reveal the presence of pockmarks (P), stratified reflectors (S), acoustically transparent zone (A), an unconformity (U), trace of mud volcano (MV), an enhanced reflector (E), pockmarked gully (Pg) that depict gas seepage activity. Along the slope three pockmarks (P) (Fig. 3b; L-6, fixes 454-455) with varying dimensions (from east to west) having 159 m, 79 m and 53 m widths and 54 m, 24 m and 15 m depths respectively are noticed. Also, identified two pockmarks (P) of rounded type and a buried gully (BG), (Fig. 3c; L-5, fixes 320-321); two slope gullies (Fig. 3d; L-4, fixes 304-305) of width 71m and 60m and depth of 3m and 2m respectively; shallow dipping reflectors (DR); traces of faults (F1-F1') (Figs. 3b and 3c), and mud volcanoes (MV). The data of entire study area was processed with a maximum penetration up to 220 m below the seafloor, characterizing the reflectors at variable thickness. An unconformable reflector (U) is seen in the figures 3a (L-7, fixes 470-471), Fig. 3d (L-4, fixes 304-305), and f (L-3). This reflector signifies surface of non-deposition, weathering or erosion that separate group of strata with continuity in deposition between them. As per the classification of Vail et al. (1984), the unconformity recorded here belongs to the second type, wherein the sub-areal surface does not reach the shelf break. Based on Gay et al. (2007), we are convinced that in the study area unconformities and pockmark relation appears to be a guiding factor for the fluid migration. We have demarcated these fault traces on to the map in Fig. 1b (F1-F1') which trends NW-SE, whereas we have also extrapolated another fault trace (F2-F2') from the recent reports (Dandapath et al 2010, 2012).

#### 3.2 Slope morphology evaluation based on the multi-beam bathymetry

Isobath intervals of 200 m are shown and profiles were chosen considering the configuration of gully, ridge and slump zones (Figs. 1a and b). The chosen thirty-three profiles constitute nine in gullies, twelve in ridge and twelve from slump zone (Fig. 1b). Multi-beam bathymetric data shows variable dimensions of the gullies

ranging from 3.72-18.6 km long, and their widths are in the range of 0.18 - 1.86 km. The spacing between the middle of the gullies typically ranges from 1.5-5.7 km, and have a maximum relief of 550 m. The slope walls of the gullies are steep towards southern ( $2.60^\circ$ ) and northern side ( $2.43^\circ$ ) respectively. The initial expression of the gullies is generally smooth negative relief with relatively gently sloping walls. The relief increases as the inter-gully areas aggrade more than the gully axis. The gullies are relatively linear features that are perpendicular to the contours and act as migration pathways for fluid flow. The transverse section (A-B in Fig. 1b) of the slope morphology is shown (Fig. 4), and corresponding profiles are portrayed (Fig. 5). The ridges (Fig. 1b) are contiguous to gullies and coalesce with each other, their length varies from 5.58 - 16.74 km, while their width in the range of 0.18-0.93 km. These ridges tend to disappear in the southern slump zone. The southern part of the slump zone occupies roughly 3352 km<sup>2</sup> area. Intermittent to these ridges and gullies we also had observed second generation gully system which are shallow interfluves and are longer than the gullies (Fig. 1b). This pattern of gullies distribution may be due to the presence of pockmarked gullies in the southern region which might have masked the actual extent of gullies here. The gradients in the study area vary within the range ( $2.13 - 3.18^\circ$ ), ( $1.19 - 4.07^\circ$ ) and ( $2.25 - 2.54^\circ$ ) for ridges, gullies, and slump zones respectively.

### *3.2.1 Correlation and principal component analysis (PCA)*

Generally, scatter plot (Fig. 6a) between the three parameters of the profiles shows prominent clustering for gullies and slumps. In particular, for slumps there is a positive correlation between the rms relief and gradients. Since rms relief is a measure of the large scale roughness it indicates that, the roughness is increasing with the slope gradients. However, reciprocity is noticed often between the rms reliefs with the depth. The relationship between the mean depth and the slope gradient is negligible for the slump zone. Gullies are characterized by the higher depth at the middle of the profile and lower at the two ends, as they are formed by the removal of soft sediment due to the bottom currents. A good correlation between the mean depth and the rms relief is observed in gully area. Gullies are characterized by gradients i.e., the roughness is high for low gradient region. Hence it can be concluded that due to the higher sedimentation rate, the gradient is reduced and rms relief is increased. The gully region having characteristically higher depth values is negatively correlated to the rms relief and positively correlated to the gradients. For ridges in the northern block, the spreading among the three parameters in the scatter plot is wide (Fig. 6a), and it is also clear that there is a considerable variation in rms relief. Hence, it is attributed that reciprocity between the rms relief and the gradient as well as mean depth are significant. Positive relationship is observed among the mean depth values and the gradient. Further, variation in the roughness with increasing mean depth is noteworthy.

To compare the performance of the three features, the PCA (principal component analysis) technique is employed. PCA is an exploratory multivariate statistics that can be used to examine data variability. Here, the PCA and scatter plot suggests that the three parameters viz. rms relief, gradients and mean depths are influencing

factors that control the profile characteristics in the ridge, gully and the slump region respectively. The PCA was used to establish the link between the above parameters and the thirty three profiles generated along three different morphological features (gradient, rms relief and depth). Gradient values and rms relief were estimated at every 100 m water depth along the profile, and the average gradient, depth, and rms relief were calculated for the entire profile length.

It is observed that the first two principal components (PC1 and PC2) together explain 94.33% of the total variance in the data. The PC1 have comparable magnitude (60.81%) subsequently PC2 and PC3 show lesser (33.52% and 5.67% respectively) values. The PCA analyses also indicate (Fig. 6b) that profiles (S1-S12) (Fig. 5) from the slump zones are consistently grouped and may represent the processes at higher depth. The same is also corroborated by the scatter plot (Fig. 6a). The biplot (Fig. 6b) reveals that the profiles in slump zones are characterized with higher depths and those of the ridges (R8-R12) from the southern area are distinctively associated with higher rms relief. However most of the profiles of the gullies (G1-G7) and ridges (R1-R7) from the northern area are characterized by their steeper gradients.

### 3.3 Stochastic multifractal fields

In our analyses, the universal form determined from  $K(q)$  expression (function of the estimated  $\alpha$  and  $C_1$ ) fits the empirical  $K(q)$  (determined from the logarithmic slopes of trace moments) (Fig. 7) quite well. A multifractal phase transition is observable in the representative plot of empirical and theoretical  $K(q)$  curves. These indicate that the measured moments will only have the theoretical  $K(q)$  for  $q$  below a critical moment  $q_c$ . Beyond  $q_c$  there is a multifractal phase transition where  $K(q)$  becomes asymptotically linear for  $q \geq q_c > 1.5$ . Indeed, for  $q < 1.5$ , the deviations from the universal form are negligible.

Estimated  $\alpha$  value ( $\approx 2$ ) of the thirty three depth profiles indicate highest degrees of multifractality. The  $C_1$  values of the thirty three profiles vary within the 0.016 - 0.1686. Overlapping trend in the variation of the  $C_1$  values for the profiles of the ridges (0.02-0.10) and gullies (0.02 – 0.10) are evident. However, profiles from the slump zones show comparatively higher values (0.03– 0.17). The lower values of  $C_1$  indicate that the profile values are close to the mean values as presented in Gagnon et al. (2006; Fig. 10). Whereas, the effect of increasing  $C_1$  indicates that, the profile data points are much deviated from their mean values. An appropriate assessment of the estimated  $\alpha$  and  $C_1$  reveals that, for higher degree of multifractality ( $\alpha \sim 2.0$ ), the  $C_1$  values are found to be within the 0.10 except for the four slope profiles (S1-S4) (Fig. 8). These four profiles, S1, S2, S3 and S4, show significantly higher  $C_1$  values i.e., 0.12, 0.11, 0.14 and 0.17 respectively. Interestingly, these profiles are situated within the proximity of the ridge and gullies towards the northern end. However, towards the southern slumping zone, profiles show comparatively lower  $C_1$  values.

Fluctuations in the estimated  $H$  values (0.78 – 1.00) are also noticed in the thirty-three bathymetric profile data. The overlapping  $H$  values of ridges, gullies and slump zones profiles are observed to be within the limits (0.81- 1.01), (0.91-1.01), and (0.78 – 0.99) respectively. Interrelationships among the  $C_1$  and  $H$  parameters for different  $\alpha$  for field values are described in Gagnon et al. (2006; Fig. 12). Accordingly, the scatter plot drawn between  $C_1$  and  $H$  indicate that the parameter combination of the twenty nine profile values lie within the  $0.02 < C_1 < 0.10$  and  $0.81 < H < 1.0$ . The combinations of the  $C_1$  and  $H$  values for remaining four profiles (S1, S2, S3, and S4 from slump zone provides (0.12, 0.80), (0.11, 0.84), (0.14, 0.78), and (0.17, 0.84) respectively. Moreover, single scatter data point which belongs to the ridge profile (R12) situated (towards the northern end) just before the S1 profile from slump zone shows ( $C_1, H$ ) as (0.10, 0.81). These five scatter points reveal that the bathymetry data possesses extremely close relationship among the thirty-three profiles.

#### 4 Discussion

We have distinctly categorized slope morphology into three types such as: gullies, ridges and slump zones using three characteristics (gradients between the two extreme points of the slope profiles, mean depth and rms roughness of the depth profile) for thirty-three high resolution multibeam depth profiles. The parameters related to ridge profiles are scattered, while the gullies and slump zones are clustered (Fig. 6a). These observations are well supported through the use of correlation results (section 3.2.1), which has also been validated using PCA studies (Fig. 6b). This indicates that the combination of rms relief, gradients and depths are well suited to distinguish the profiles between the ridge, gully and the slump regions. The two principal components (PC1 and PC2) together explain 94.33% of the total variance. The PC1 has comparable magnitude (60.81%), whereas the PC2 depicts lesser (33.52%). The PCA analyses also indicate that the slump zone profiles (S1-S12) are consistently grouped (Fig. 6b) as an entity. The biplot (Fig. 6b) reveals that the profiles in the slump zones are characterized by higher depths and those of the ridges (R8-R12) from the southern area (Fig. 1b) are distinctly associated with higher roughness. While, most of the remaining profiles of the gullies (G1-G7) and ridges (R1-R7) from the northern area are characterized by their gradients.

We presume that there is a presence of slumping or material flow associated with the four profiles (S1-S4) and the single ridge profile (R12) (Fig. 1b). Interestingly, such information could not be explained from the scatter plots alone including the PCA. Therefore, in order to resolve this issue, we utilized a stochastic multifractal technique, which has advantages to address the intermittency in the framework of higher-order nonlinear dynamical system. Here, three distinct parameters were used to understand this system, which are easier to comprehend the multifractality (i.e., high dimensionality), and signifying more suitability in defining fine-scale seafloor aspects (Chakraborty et. al. 2013). The  $\alpha$  values of the bathymetry profiles show identical trend ( $\approx 2$ ), expressing similar degree of multifractality of the thirty-three profiles. The scatter plot between the parameters  $C_1$  and  $H$  suffice the required fine-scale information (Fig. 8). The lower values of  $C_1$  attributed to the twenty-eight

profiles indicating that the field values are close to the mean values. However, for remaining five profiles (S1-S4 and R12) the field values are fluctuating with respect to the mean values because of the higher  $C_1$  values. Except for the S1-S4 and R12 profiles, higher values of  $H$  parameter show smoothness of the twenty-eight profiles (Fig. 5).

As already mentioned that the slumping on the WCMI was effected till the 11ky B.P. (Hussain and Guptha 1985), and the magnitude of the slumping is minimal thereafter. Despite this, it is believed that the formation of methane gas during the Holocene might have also triggered the small scale process of slumping. This led us to think that after sea level attaining the present scenario, apparently large scale slumping might not have been taken place. However, the characteristic slump zone in the study area (Fig. 1b) with the presence of gas escape features is an additional point to ponder over the relevance of this slumping. In this regard, Guptha et al. (2002) had shown that the methane-bearing gas charged sediments (Karisiddaiah et al. 1993) might be the main cause of the slumping. Thus, the presence of pockmarks in the region and their detailed morphological characteristics (e.g., shape, sidewall slope etc.) had also strengthened such possibilities of slumping (Dandapath et al. 2010; 2012). Further, we speculate that the vertical rising of gas bubbles and gravitational pulls along the sidewall of the pockmarks might have initiated slumping. Similar events due to upward migration of gas were also recorded (Ergün et al. 2002). Overall, the slope area with the dominant pockmark seepages coupled with the fault traces clearly reflect a structurally weak zone (Figs. 1b and 2). Main controlling factor of slump appears to be due to the dissociation of adjacent deep-seated gas hydrate zones (Fig. 1a) as reported by Rao et al (2001).

The presence of gully and ridges in the slope region may be related to the Holocene turbidite events. However, these gullies appear to be spread more to the northern part of the study area, but the southern slump zone is either masked or very few such features which render more erosional. Hence, we presume that the source for such erosional processes may possibly be related to the dominant poleward bottom currents off Goa slope region (during the winter monsoon) than the weaker equatorward bottom currents (during the summer monsoon) (Amol et al. 2012). In general, for WCMI slope region under study, the magnitude of bottom currents is higher towards the south (Bhatkal in Karnataka) than the north (Jaigarh in Maharashtra). Interestingly, off Goa slope falls within these two areas, and cross section of the profiles along 600m contour depicts strong erosional effect in the southern part of the slump zone (Fig. 4). Whereas the effect of erosion is minimal towards the north such that the gully and ridge features are found to be intact. The stochastic multifractal based estimated values show higher  $C_1$  (sparseness) and lower  $H$  (smoothness) between the gully / ridges and slump zone (Figs. 1b and 4). The S1-S4 profile (~ 20km length) characteristics from the slump zone show variations around the mean value (higher  $C_1$ ) are dominant and relief roughness is higher (lower  $H$ ) (Figs. 1b and 4). And  $C_1$  and  $H$  values from remaining areas (gullies, ridges and slump zones) forms separate cluster pattern (Fig. 8). Therefore, we presume that the convoluted nature of the slope containing the four profiles (S1-S4) that tend to change gradually to the extent that

they may diminish at a later stage due to the interaction between the diverse pole/ equatorward current patterns in association with the inherent geodynamic fabric of the slope. We had come across very few pockmarked gullies (Pg; Fig. 3e, L-3) in the study area. These are slightly different from the other gullies as the former ones are the fluid flow conduits. We consider these gullies formed through the interaction of slope failure and fluid escape processes (Pilcher and Argent, 2007). Their presence in the southern area strengthens the view that probably this area is partly devoid of gullies, even though Fig. 5 depicts their presence. We had noticed an affinity between pockmark (P) and gullies in the form of fluid flow systems like few traces of mud volcanoes (MV) (Fig. 3c and 3f) and enhanced reflectors (E), (Fig. 3f). Similar work has been reported elsewhere (Field et al. 1999; Moss et al 2012). Further we believe that pockmarks (as reported by Dandapath et al 2010, close to the study area) are related to gullies and thus might acted as preferred escape routes for the migration of gas. The association of offshore currents and negative and positive geomorphic features is not an uncommon feature. In this regard it is pertinent to refer the work of Leon et al (2006) from offshore Moroccan (Gulf of Cadiz) continental margin the occurrence of offshore currents and their effect on the formation of mud volcanoes and pockmarks.

## 5 Conclusions

The morphological characteristics of the WCMI, off Goa, display varying slope angles for the gullies and ridges, while it is comparable in the slump zone from north to south. The seismic construal explains the presence of gas-charged sediments, gas-escape features in the form of fluid flow systems such as pockmarks, mud volcanoes, enhanced reflectors and pockmarked gullies in the study area. The scatter plot involving average slope gradient, rms relief, and mean depth of the thirty-three profiles depict unsettled huddling of the ridge profiles whereas the gullies and the slump zones show good clustering. These observations were validated using PCA. However, the presence of slump or material flow along the four profiles (S1-S4) in the slump zone and the single ridge profiles (R12) that has been depicted within the mapped area (Fig. 1b) could not be explicated by means of the scatter plots and PCA. Therefore, we had to take recourse to stochastic multifractal technique in order to identify the slumping through the estimation of three parameters such as:  $\alpha$  (degree of multifractality),  $C_1$  (sparseness),  $H$  (smoothness). The degree of multifractality ( $\alpha \sim 2$ ) is found to be the highest for all the studied profiles. The parameters show higher  $C_1$  (sparseness) and lower  $H$  (smoothness) between the gully / ridges and slump zone profiles. It generally means that, except S1-S4 profiles and nearby ridge (R12) area ( $\sim 20$ km length) between the gully / ridges and slump zone, remaining parameters of the twenty-eight depth profiles show minimum variations around the mean values (lower  $C_1$ ) and lesser relief roughness (higher  $H$ ). However,  $C_1$  and  $H$  values from these gullies, ridges and slump zones form a separate cluster pattern. Interestingly, the study area holds fault traces (Fig. 1b) along with the dominant pockmark seepages indicating a structurally weak zone. Sun et al (2012) reports that structures that are indicative of focused fluid flow, such as seismic chimneys, mud diapirs, mud volcanoes, pipes, faults, sand injections and pockmarks, are wide spread in passive and active

continental margins, and they have received increasing attention over the last decade due to the wider appreciation of their importance for understanding fluid flow in sedimentary basins. They are also being investigated because of their role in assessing seabed stability. The presence of gullies and ridges in the slope region seem to be connected with the Holocene turbidite events. These gullies appear to be confined within the northern part of the study area. Interestingly the southern slump zone has rendered itself to erosional processes. Hence, we can deduce that the source for such erosional activities may possibly be connected with the dominant poleward bottom currents in the slope region off Goa (during the winter) and the weakened equatorward bottom currents (during the summer monsoon). The slender narrowing of the shelf (15° 50' N - 16°N) changes the aspect of the slope containing the four profiles (S1-S4). The diverse current patterns and the unique seafloor topography portend gradual changes in dislocating the inherent slope morphology.

### **Acknowledgements**

The authors thank Dr. S. W. A. Naqvi, Director, National Institute of Oceanography for permitting publication of this work, and Dr. P. S. Rao for his help in many ways. We place on record our thanks to all the anonymous reviewers for their meticulous comments on our earlier version. We are also thankful to the Ministry of the Earth Sciences, New Delhi for their support. K. Haris expresses his thanks to CSIR for the grant of fellowship. We place on record and dedicate this contribution to late Dr. VN Kodagali, an established researcher in the field of multibeam bathymetry who is no more now. This is NIO contribution xxxx.

### **References**

- Adams EW, Schlager W (2000) Basic types of submarine slope curvature. *J Sed Res* 70: 814-828
- Amol P, Shankar D, Aparna SG, Shenoj SC, Fernando V, Shetye SR, Mukherjee A, Agervadekar Y, Khalap S, Satelkar NP (2012) Observational evidence from direct current measurements for propagation of remotely forced waves on the shelf off the west coast of India. *J Geophys Res* 117: C05017. doi:10.1029/2011/2011JC007606, 2012
- Bhattacharyya R, Verma PK, Majumdar TJ I (2009) High resolution satellite geoids/gravity over the western Indian offshore for tectonics and hydrocarbon exploration. *Indian J Mar Sci* 38:116-125
- Bhattacharya GC, Chaubey AK (2001) Western Indian Ocean e a glimpse of the tectonic scenario. In: Gupta RS, Desa E (eds) *The Indian Ocean – A Perspective*. Oxford-IBH, New Delhi, pp. 691-729
- Bøe R, Rise L, Ottesen D (1998) Elongate depressions on the southern slope of the Norwegian Trench (Skagerrak) : morphology and evolution. *Marine Geol* 146:191-203
- Chakraborty B, Haris K, Latha G, Maslov N, Menezes A (2014) Multifractal Approach for Seafloor Characterization. *IEEE Geosci Remote Sens Lett* 11(1); 54-58. doi: 10.1109/LGRS.2013.2245856

- Chakraborty B, Mukhopadhyay R, Jauhari P, Mahale V, Shashikumar K, Rajesh M (2006) Fine-scale analysis of shelf–slope physiography across the western continental margin of India. *Geo-Mar Lett* 26: 114–119. doi: 10.1007/s00367-006-0022-6
- Cheng Q, Agterberg FP (1996) Comparison between two types of multifractal modeling. *Math Geol* 28 (8): 1001–1015
- Dandapath S, Chakraborty B, Maslov N, Karisiddaiah SM, Ghosh D, Fernandes W, Menezes A (2012) Characterization of seafloor pockmark seepage of hydrocarbons employing fractal: A case study from the western continental margin of India. *Marine Petrol Geol* 29: 115-128
- Dandapath S, Chakraborty B, Karisiddaiah SM, Menezes AA, Fernandes W, Naik DK, Prudhvi Raju KN (2010) Morphology of pockmarks along the western continental margin of India: Employing multi-beam bathymetry and backscatter data. *Marine Petrol Geol* 27(10): 2107-2117
- Davis JC (1973) *Statistics and Data Analysis in Geology*. John Wiley & Sons, Newyork, pp 412-536
- Dimri VP (2005) Fractals in geophysics and seismology: an introduction. In: Dimri VP (ed) *Fractal Behaviour of the Earth System*. Springer-Verlag, Berlin, pp 1-22
- Dowdeswell JA, Cofaig CO, Noormets R, Larter RD, Hillenbrand CD, Benetti S, Evans J, Pudsey CJ (2008) A major trough-mouth fan on the continental margin of the Bellingshausen Sea. West Antarctica: The Belgica Fan. *Marine Geol* 252:129-140. doi:10.1016/j.margeo.2008.03.017
- Ergün M, Dondurur D, Çifçi G (2002) Acoustic evidence for shallow gas accumulations in the sediments of the eastern Black Sea. *Terra Nova* 14:313-320
- Farre JA, McGregor BA, Ryan WBF, Robb JM (1983) Breaching the shelfbreak; Passage from youthful to mature phase in submarine canyon evolution. In: Stanley DJ, Moore GT (eds) *The shelfbreak: critical interface on continental margins*. Soc Econ Palaeontol Mineral Special Publications 33:25–39
- Field ME, Gardner JV, Prior DB (1999) Geometry and significance of stacked gullies on the northern California slope. *Marine Geol* 54: 271-286
- Fox CG, Hayes DE (1985) Quantitative methods for analyzing the roughness of the seafloor. *Rev Geophys* 23: 1-48
- Gay A, Lopez M, Berndt C, Séranne M (2007) Geological controls on focused fluid flow associated with seafloor seeps in the Lower Congo Basin. *Marine Geol* 244: 68– 92
- Goff JA (2001) Quantitative classification of canyon systems on continental slopes and a possible relationship to slope curvature. *Geophys Res Lett* 28(23): 4359-4362
- Green AN, Goff J, Uken RU (2007) Geomorphological evidence for upslope canyon-forming processes on the northern Kwazulu-Natal shelf, SW Indian Ocean, South Africa. *Geo-Marine Lett* 27: 399-409
- Gagnon JS, Lovejoy S, Schertzer D (2006) Multifractal earth topography. *Nonlin Processes Geophys* 13: 541–570
- Guptha MVS, Mohan R, Muralinath AS (2002) Slumping on the western continental margin of India. *GeoActa* 1: 45-48
- Halsey TC, Jensen MH, Kadanoff LP, Procaccia I, Shraiman BI (1986) Fractal measures and their singularities: The characterization of strange sets. *Phys Rev A* 33 (2): 1141–1151
- Hentschel HGE, Procaccia I (1983) The infinite number of generalized dimensions of fractals and strange attractors. *Physica D* 8: 435-444

- Hernandez-Molina FJ, Ercilla D, Van Rooij D (2011) Along-slope oceanographic processes and sedimentary products around the Iberian margin. *Geo-Mar Lett* 31: 315-341
- Hewlett JS, Jordan DW (1993) Stratigraphic and combination traps within a seismic sequence framework, Miocene Stevens turbidites, Bakersfield Arch, California. In: Weimer P, Posamentier H (eds) *Siliciclastic Sequence Stratigraphy: American Association of Petroleum Geologists (AAPG) Memoir 58*, pp 135–162
- Hovland M, Gardner JV, Judd AG (2002) The significance of pockmarks to understanding fluid flow processes and geohazards. *Geofluids* 2: 127-136.
- Hussain N, Gupta MVS (1985) Ooids in a deep sea core from the western continental margin of India. *Indian J Mar Sci* 14:123-126
- Karisiddaiah SM, Veerayya M, Vora KH, Wagle BG (1993) Gas-charged sediments on the inner continental shelf off western India. *Mar Geol* 110: 143-152
- Karisiddaiah SM, Veerayya M, Vora KH (2002) Seismic and sequence stratigraphy of the central western continental margin of India: late-Quaternary evolution. *Mar Geol* 192: 335-353
- Kodagali VN, Chakraborty B (1994) Performance appraisal of multibeam systems-Hydrosweep at different seabed provinces. In: Sushilkumar, Agadi VV, Das VK, Desai BN (eds) *Ocean Technology Perspectives Publ Inform Directorate New Delhi, India* pp 335-346
- Lastras G, Canals M, Urgeles R, Amblas D, Ivanov M, Droz L, Dennielou B, Fabrés J, Schoolmeester T, Akhmetzhanov A, Orange D, García-García A (2007) A walk down the Cap de Creus canyon, northwestern Mediterranean Sea: recent processes inferred from morphology and sediment bedforms. *Mar Geol* 246: 176–192
- Leon R, Somoza L, Medialdea T, Maestro A, Díaz-del-Río V, Fernández-Puga MC (2006) Classification of sea-floor features associated with methane seeps along the Gulf of Cadiz continental margin. *Deep-Sea Res II* 53: 1464–1481
- Lovejoy S, Schertzer D (2007) Scaling and multifractal fields in the solid earth and topography. *Nonlin Proc Geophys* 14 (4): 465-502
- Lovejoy S, Schertzer D, Allaire V, Bourgeois T, King S, Pinel J, Stolle J (2009) Atmospheric complexity or scale by scale simplicity? *Geophys Res Lett* 36: L01801. doi:10.1029/2008GL035863
- Maillet GM, Vella C, Berne S, Friend PL, Amos CL, Fleury TJ, Normand A (2006) Morphological changes and sedimentary processes induced by the December 2003 flood event at the present mouth of the Grand Rhone River (southern France). *Mar Geol* 234(1–4): 159–177. doi: 10.1016/j.margeo.2006.09.025
- Mandelbrot BB (1989) Multifractal measures, especially for the geophysicist. *PAGEOPH* 131(1/2): 5-42
- Mitchell NC (2005) Interpreting long profiles of canyons in the USA Atlantic continental slope. *Mar Geol* 214: 75-99. doi:10.1016/j.margeo.2004.09.005
- Moss JL, Cartwright J, Moore R (2012) Evidence of fluid migration following pockmark formation: Examples from the Nile deep sea fan. *Mar Geol* 303-306 (1-13).
- Mukhopadhyay R, Rajesh M, De S, Chakraborty B, Jauhari P (2008) Structural highs on western continental slope of India: Implications for regional tectonics. *Geomorphology* 96 (1-2): 48-61
- Naqvi SWA, Bange HW, Farias L, Monteiro MS, Scranton MI, Zhang J (2010) Marine hypoxia/anoxia as a source of CH<sub>4</sub> and N<sub>2</sub>O. *Biogeosciences* 7: 2159-2190

- O'Grady DB, Syvitski JPM, Pratson LF, Sarg JF (2000) Categorizing the morphologic variability of siliciclastic passive continental margins. *Geology* 28: 207-210
- Pilcher R, Argent J (2007) Mega-pockmarks and linear pockmark trains on the West African continental margin. *Mar Geol* 244: 15–32
- Reineck HE, Singh IB (1980) *Depositional Sedimentary Environments*, second ed. Springer-Verlag, Berlin. 549pp
- Rao PS, Rao CHM, Reddy NPC (1988) Pyritized ooids from the Arabian Sea Basin. *Deep Sea Res* 35:1215-1221
- Rao YH, Subrahmanyam C, Rastogi A, Deka B, (2001). Anomalous features related to gas/gas hydrate occurrences along the western continental margins of India. *Geo Mar Lett* 21: 1-8
- Shetty MGAP (1972) A description of sediment cores from the Arabian Sea. *Proceedings International Geology Congress* 8:109-119
- Schertzer D, Lovejoy S (1987) Physical Modeling and Analysis of Rain and Clouds by Anisotropic Scaling Multiplicative Processes. *J Geophys Res* 92(D8):9693-9714
- Seuront L, Schmitt F, Lagedeuc Y, Schertzer D, Lovejoy S (1999) Universal multifractal analysis as a tool to characterize multiscale intermittent patterns: example of phytoplankton distribution in turbulent coastal waters. *J Plankton Res* 21(5):879-922
- Shetye SR, Gouveia AD, Shenoi SSC, Sundar D, Michael GS, Almeida AM, Santanam K (1990) Hydrography and circulation of the west coast of India during the southwest monsoon 1987. *J Mar Res* 48: 359-378
- Singh AP, Mishra OP, Rastogi B K, Kumar D (2011). 3-D Seismic Structure of the Kachchh, Gujarat and its Implications for the Earthquake Hazard Mitigation, *Nat Haz* 57(1): 83-105
- Spinelli GA, Field ME (2001) Evolution of continental slope gullies on the northern California margin. *J Sediment Res* 71(2): 237–245
- Stackelberg UV (1972) Faziesverteilung in sedimenten des Indisch-Pakistanischen Kontinentalrandes ‘Meteor’ *Forschungsergebnisse* 9:1-73
- Stow DAV, Hernandez-Molina FJ, Llave E, Sayago M, Diaz del Rio V, Branson A (2009) Bedform-velocity matrix: the estimation of bottom current velocity from bedform observations. *Geology* 37(4): 327-330
- Sun Q, Wu S, Cartwright J, Dong D (2012) Shallow gas and focused fluid flow systems in the Pearl River Mouth Basin, northern South China Sea. *Mar Geol* 315-318:1-14
- Syvitski JP, Alexander CR, Field ME, Gardner JV, Orange DL, Yun JW (1996) Continental slope sedimentation: The view from northern California: *Oceanography* (Washington, DC), 9: 163–167
- Vail PR, Hardenbol J, Todd RG (1984) Jurassic unconformities, chrono-stratigraphy, and sea level changes from seismic stratigraphy and biostratigraphy. In: Schlee JS (ed) *Interregional unconformities and hydrocarbon accumulation*. AAPG Mem 36: 129-144
- Weaver PPE, Wynn RB, Kenyon NH, Evans J (2000) Continental margin sedimentation, with special reference to the north-east Atlantic margin. *Sedimentology* 47: 239–256

## Figure captions

**Fig 1:** (a) Study area location including some of the main structural features (adapted from Dandapath et al. 2012) of the region. On land the Dharwarian trend shown by dotted lines is the NNW-SSE trending Precambrian orogenic structure. The west coast fault shown with thick dotted lines is different from the Dharwar trend. Red highlighted lines and grey shade indicate the reported BSR (bottom simulating reflectors) zone (Dandapath et al. 2010). Traces of two faults are marked as F1-F1', and F2-F2'. (b) View of the study area in 3D (Fig. 2), and the representative seismic sections (6 black lines) explained in detail in Fig. 3. The locations of thirty-three profiles (Fig. 4) of gullies (G1-G9), ridges (R1-R12) and slump zones (S1-S12) are shown. The northern area is composed of visibly characteristic gullies and intervening ridges, whereas the southern area is with little visible gullies, however interfluves of second generation gullies are observed here. NW-SE trending line A-B (red in color) represents a schematic view of the gullies, ridges and slope zone studied (Fig. 5). The contour interval is 200 m.

**Fig 2:** Perspective view of the study area showing characteristics of gullies, ridges and slump zones. Location of studied pockmarks (P, Pg), mud volcano (MV), two faults (F), gullies (G) are shown along with ridges and slump collectively. **AB** represents a northwest-southeast trending profile cutting gullies, ridges and slump zone. Fix nos. are given as numerals (162 ...169... 471). Thin redlines L-3...7 are the seismic lines studied.

**Fig 3:** Single channel (4.5 -8 kJ) seismic reflection profiles in the study area off Goa: (a) A cross section of Line 7 (L-7) (between fixes 470-471) showing typical slope region with stratified reflectors (S), dipping reflectors (DR) and an unconformity (U) at a depth of ~25m bsf (below seafloor) conspicuously demarcating the sequence boundary of top reflector with the underlying stratified layers. (b) A transect of Line 6 (L-6) showing typical cross section of three pockmarks (P) with variable dimensions (see text), note both dipping (DR) as well as deep reflectors (D). Maximum penetration is up to 350 bsf. (c) A small portion of Line 5 (L-5) showing two pockmarks (P) of rounded type, a buried gully (BG), shallow dipping reflectors (DR), traces of faulting (F1-F1'), mud volcanoes (MV), an acoustically transparent zone (A) and deep reflectors (D); M indicates multiple reflector. (d) This section of Line 4 (L-4) depicts a cross view of two slope gullies that appear as faulted, together with dipping reflectors (DR), an unconformity (U) and deep stratified reflectors (S). (e) A small portion of Line 3a (L-3a) from the southernmost slump zone shows stratified reflectors (S), acoustically transparent zone (A), an unconformity (U), trace of mud volcano (MV), and an adjacent enhanced reflector (E). (f) Another small stretch of Line 3b (L-3b) from deeper portion shows a pockmarked gully, depicting gas seepage activity along with stratified reflectors (S). X denotes the gap in seismic data recording for 15 minutes, depicting changes in topography, resulting in artifact (and not a fault).

**Fig 4:** A composite diagram showing thirty-three depth profiles from the study area comprising of gullies (G1-G9), ridges (R1-R12) and slump zone (S1-S12). Representative undulating slump zone profiles (S1-S4) are indicated as (1), and remaining slump zone profiles (S5-S12) is represented by (2), whereas (3) and (4) represent ridge and gully profiles respectively.

**Fig. 5:** A schematic line diagram A-B describing in detail all the ridges, gullies and slumps across the chosen profiles. For profile locations please see Fig. 1 (b).

**Fig. 6:** (a) Scatter plot drawn considering mean water depth, gradients and rms relief of all the thirty-three profiles. (b) Figure represents the biplot which reveals that the profiles in the slump zones are characterized by higher depths and those of the ridges (R8-R12) from the southern area are distinctly associated with higher roughness. While, most of the remaining profiles of the gullies (G1-G7) and ridges (R1-R7) from the northern area are influenced by their gradients.

**Fig. 7:** Scaling behavior of the statistical moments of the representative ridge, gully and slump is illustrated here by the straightness of the Log/log curves of the normalized trace moment as functions of the scale ratio  $\lambda=L/l$ . The values of the exponent  $q$  of each trace moments vary between 0 and 2.

**Fig. 8:** Scatter plot of profile wise multifractal parameters estimated using stochastic multifractal formalism. The values associated with the slump S1-S4 are encircled.

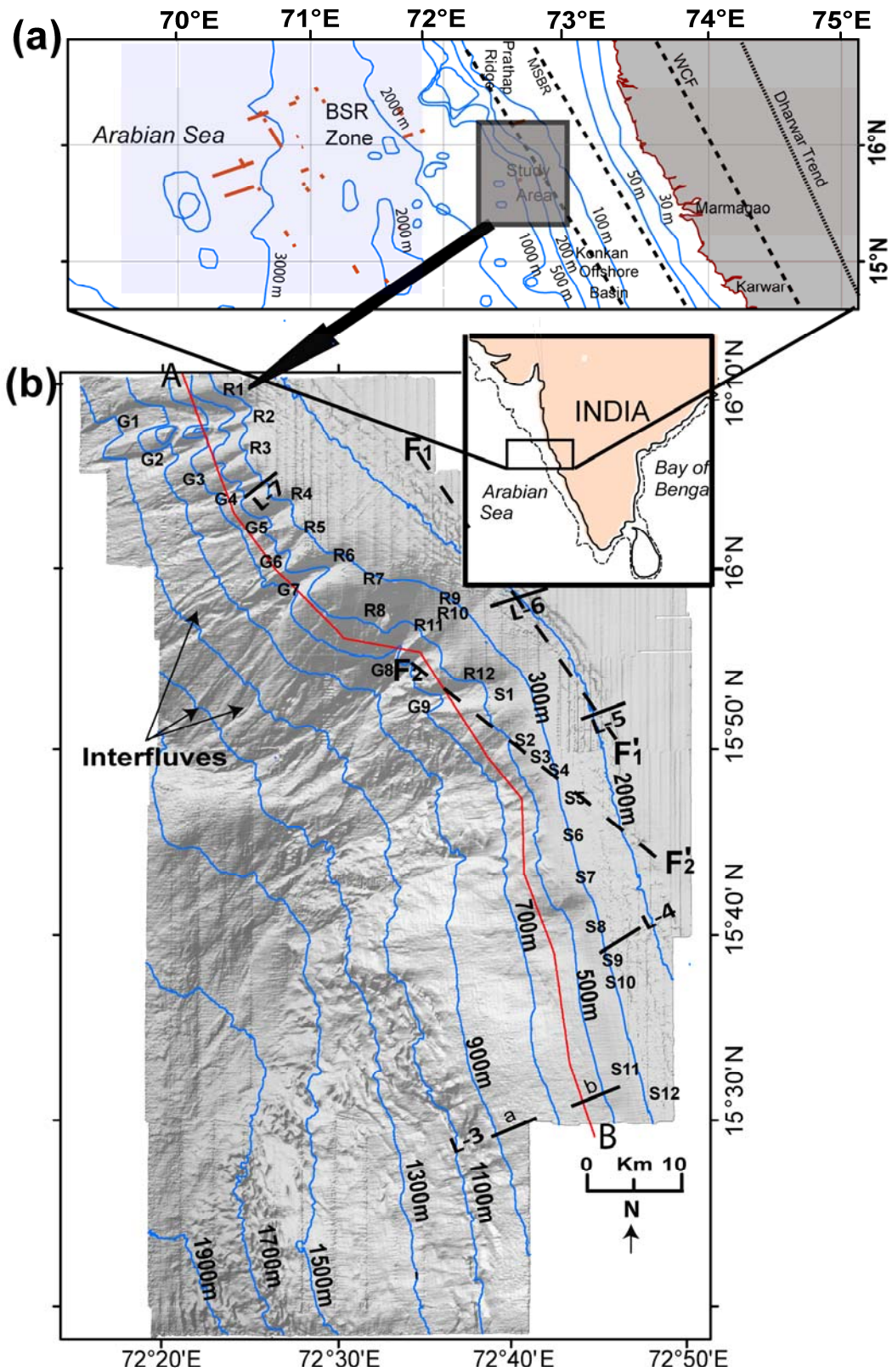


**Fig. 1**

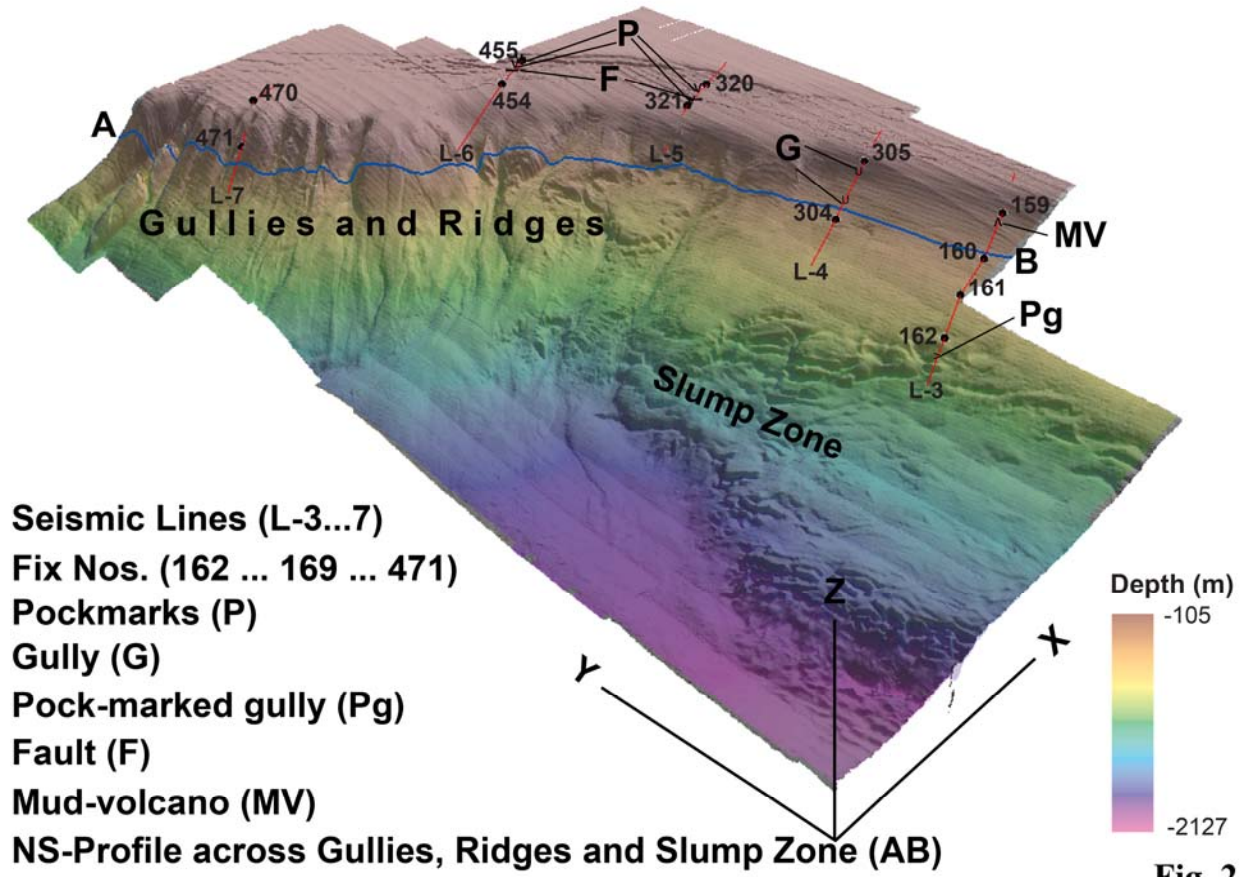


**Fig. 2**

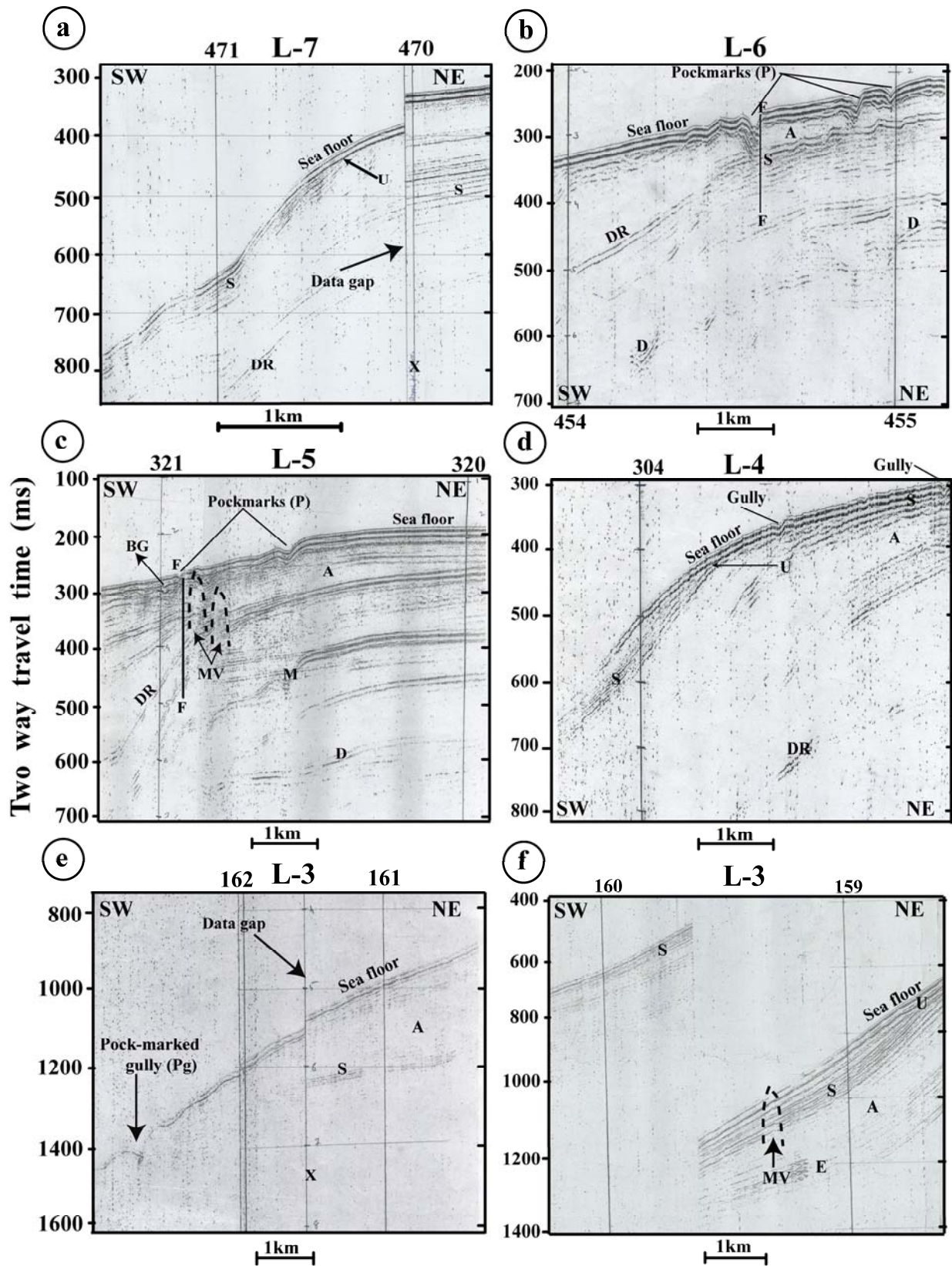


Fig. 3

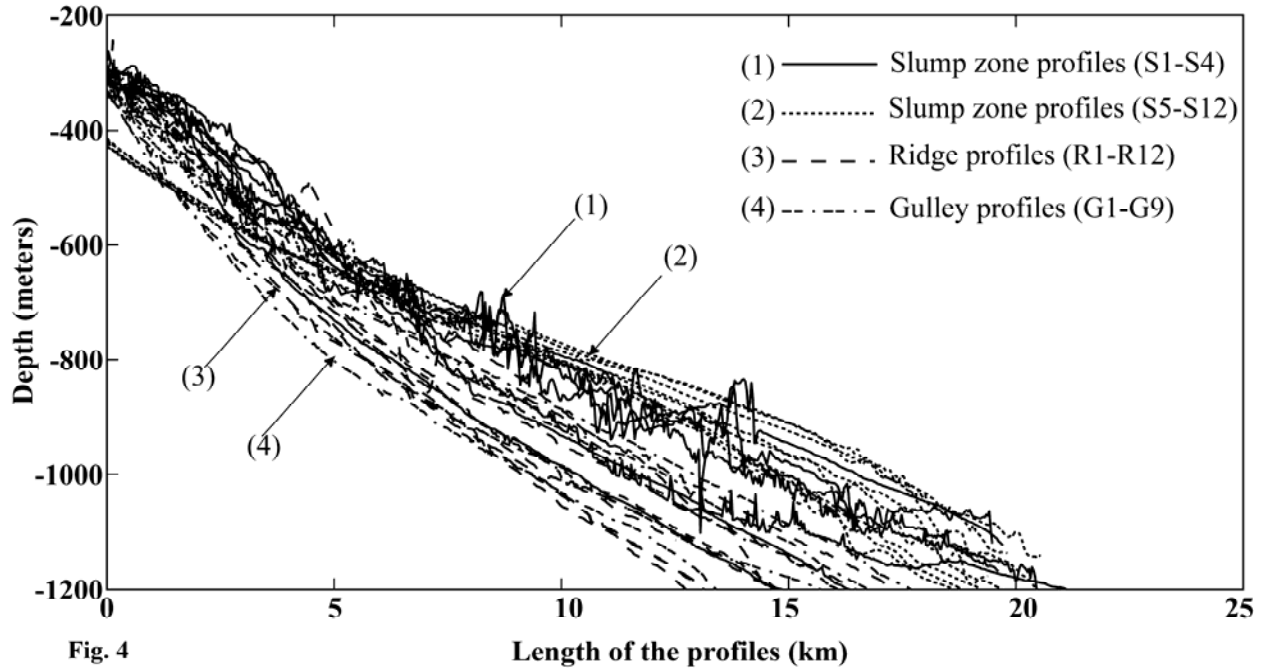


Fig. 4

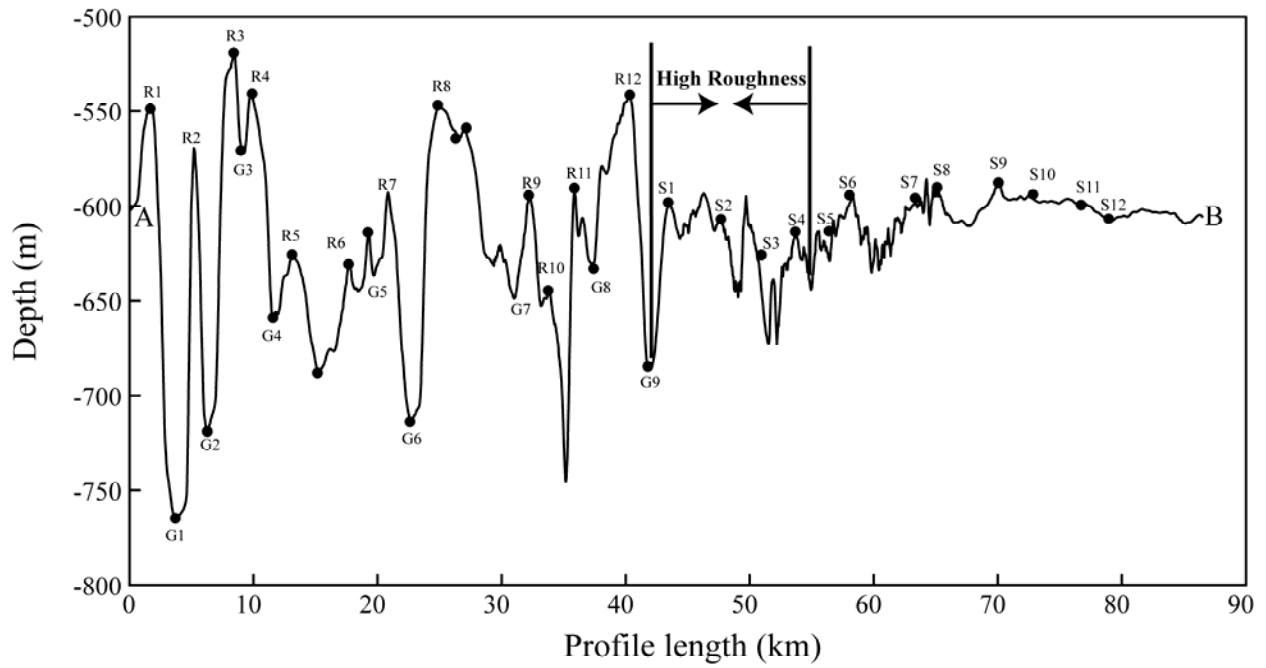


Fig. 5

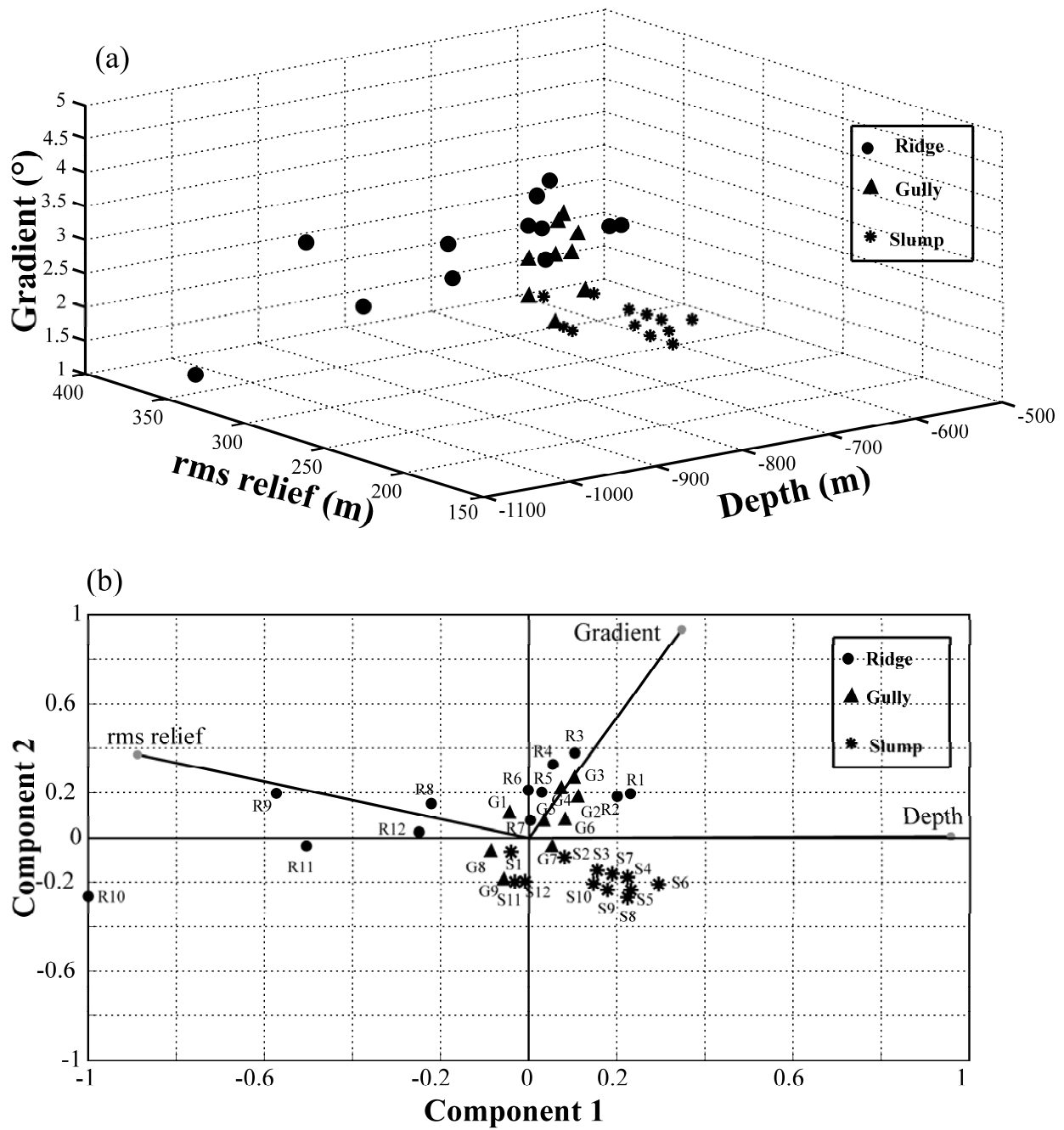


Fig. 6

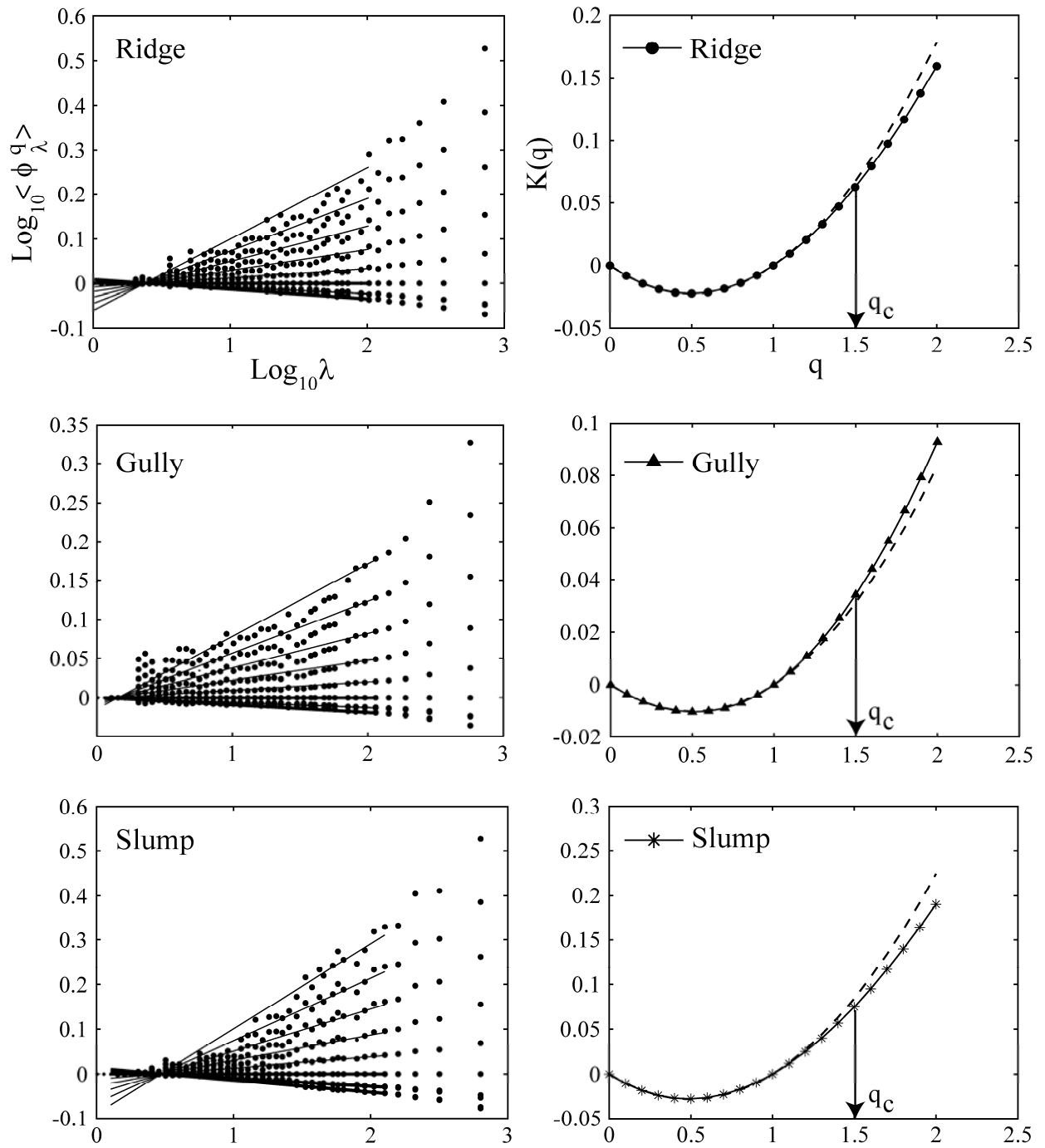


Fig. 7

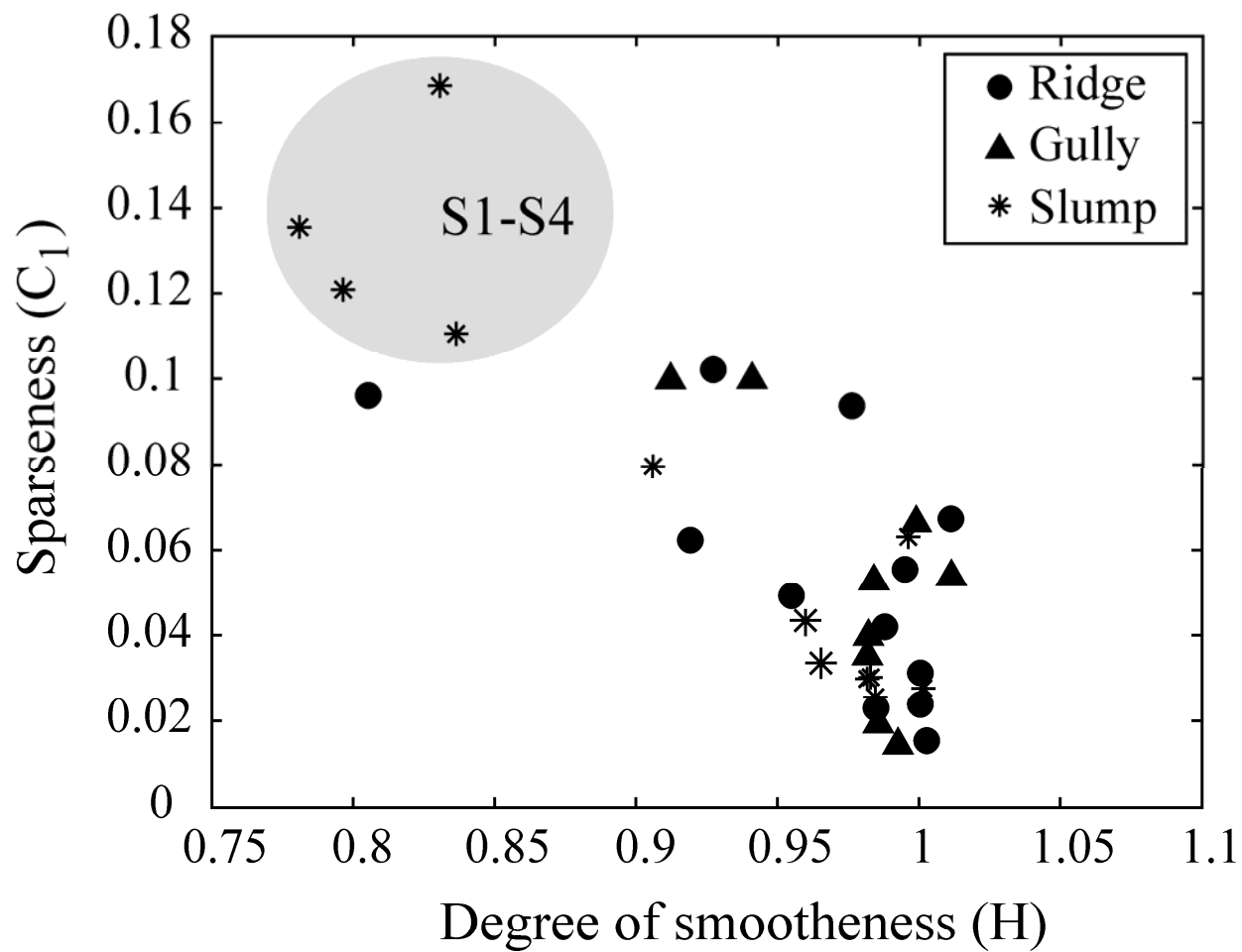


Fig. 8